Detecting low-frequency earthquakes within non-volcanic tremor in southern Taiwan triggered by the 2005 Mw8.6 Nias earthquake

Chi-Chia Tang,[1,2] Zhigang Peng,[2] Kevin Chao,[2] Chau-Huei Chen,[1] and Cheng-Horng Lin[3]

[1] We use a matched filter technique to detect 41 low-frequency earthquakes (LFEs) within 700-s of triggered tremor signals in the Southern Central Range in Taiwan during the surface waves of the 2005 Mw8.6 Nias earthquake off the coast of northern Sumatra. The depth distributions of LFEs after double-difference relocations concentrate at the depth range of 12–38 km below the background seismicity and above the Moho depth inferred from receiver function studies. The locations of LFEs are close to the downward extension of the steep-dipping Chaochou-Lishan fault with only modestly high Vp/Vs ratios (1.75–1.85). Our observation indicates that at least portions of triggered tremor consists of many LFEs, similar to ambient tremor observed at other major plate boundary faults. **Citation:** Tang, C.-C., Z. Peng, K. Chao, C.-H. Chen, and C.-H. Lin (2010), Detecting low-frequency earthquakes within non-volcanic tremor in southern Taiwan triggered by the 2005 Mw8.6 Nias earthquake, *Geophys. Res. Lett.*, *37*, L16307, doi:10.1029/2010GL043918.

1. Introduction

[2] Deep "non-volcanic" tremor is a subtle seismic signal with long durations and no clear body wave arrivals observed away from volcanic regions [*Obara*, 2002]. Tremor often accompanies slow-slip events, and together they are termed "episodic tremor and slip" [*Rogers and Dragert*, 2003]. Tremor has been found at many places along the circum-pacific subduction zones and the transform plate boundary in California [*Rubinstein et al.*, 2010; *Peng and Gomberg*, 2010, and references therein]. Tremor appears to be highly stress sensitive, and can be triggered instantaneously by the passing surface waves [e.g., *Rubinstein et al.*, 2007; *Peng and Chao*, 2008; *Peng et al.*, 2009].

[3] Because of the lack of clear P- and S-wave arrivals in the near continuous tremor episodes, obtaining an accurate location of tremor, especially the depth, has been difficult [e.g., *Kao et al.*, 2009; *Rubinstein et al.*, 2010]. Recent studies have shown that tremor consists of many low-frequency earthquakes (LFEs) with weak P and S waves and deficient in high-frequency energy [*Shelly et al.*, 2007]. This provides a new approach for accurate tremor location, especially the depth [*Brown et al.*, 2008, 2009], and hence improves our knowledge of the underlying physical mechanism of tremor and LFE generation.

[4] In this study we apply the recently developed matched filter technique [*Gibbons and Ringdal*, 2006; *Shelly et al.*, 2007; *Brown et al.*, 2008, 2009; *Peng and Zhao*, 2009] to detect LFEs within tremor in Southern Taiwan triggered by the 28 March 2005 Mw8.6 Nias earthquake (Figure 1). This study is built upon our recent findings of tremor triggered by surface waves of large teleseismic events beneath the Central Range (CR) in Taiwan [*Peng and Chao*, 2008; K. Chao et al., Remote triggering of non-volcanic tremor around Taiwan, submitted to *Geophysical Journal International*, 2010]. The tremor triggered by the 2005 Nias earthquake is one of the most clearly recorded episodes (Figures 2 and S1) and hence is further studied here.[1]

2. Data and Method

[5] We examined waveform data during the passage of large-amplitude surface waves of the 2005 Mw8.6 Nias earthquake recorded by 4 stations in the Broadband Array in Taiwan for Seismology (BATS) and 9 short-period stations in the Central Weather Bureau Seismic Network (CWBSN) (Figure 1). The great circle distance and the back-azimuth to the BATS station TPUB are 3453 km and 231°, respectively. We first cut the data between 900 s and 1600 s after the occurrence time of the mainshock, removed the mean, re-sampled the data to 20 samples/s, and then applied a 2–8 Hz band-passed filter. The high-frequency tremor signal is coherent among many stations with the moveout close to that for the S waves (Figure 2a), and is in phase with the passing surface waves of the teleseismic event (Figure S1).

[6] Next we visually identified 11 LFEs within the entire 700-s of tremor bursts with relatively high signal-to-noise ratios (SNR) and clear P and S arrivals (Figure S2), and manually picked the P- and S-wave arrivals at nearby stations with high waveform similarities (Figure S3). Then we located them by a double-difference algorithm [*Waldhauser and Ellsworth*, 2000] according to the 1-D velocity model (Table S1) of central Taiwan [*Chen et al.*, 2001]. The same model has been used to locate tremor in our previous studies [*Peng and Chao*, 2008; K. Chao et al., submitted manuscript, 2010]. Next, we created an averaged 1-D model (Table S2) from the recent 3D velocity model of *Wu et al.* [2007] based on the box that bounds the initial location of the 11 LFEs (Figure S4). The 11 LFEs are relocated according to the new 1-D velocity model (Figures S5 and S6). Finally we calculated the theoretical S-wave

---

[1]Institute of Seismology, National Chung Cheng University, Min-Hsiung, Taiwan.
[2]School of Earth and Atmospheric Sciences, Georgia Institute of Technology, Atlanta, Georgia, USA.
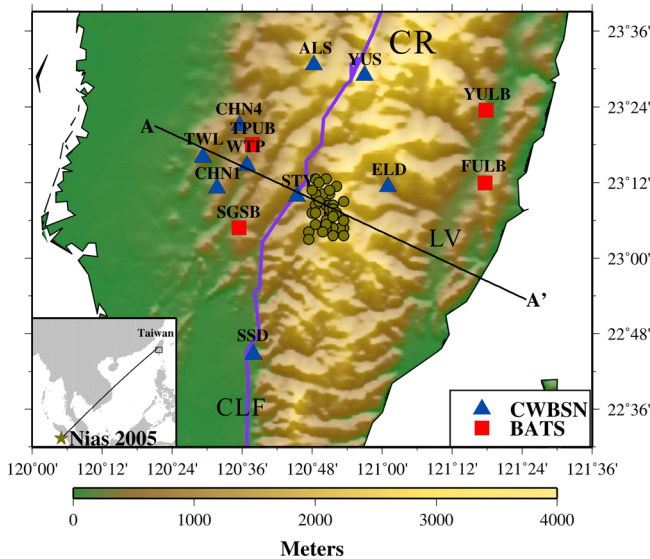[3]Institute of Earth Sciences, Academia Sinica, Taipei, Taiwan.

Figure 1. Locations of low-frequency earthquakes (dark green circles) within tremor triggered by the passing surface waves of the 28 March 2005 Mw8.6 Nias earthquakes. Squares and triangles represent the stations used in this study within the Broadband Array in Taiwan for Seismology (BATS) and the Central Weather Bureau Seismic Network (CWBSN), respectively. The cross section line AA' marks the direction perpendicular to the Central Range (CR). The blue line marks the surface expression of the Chaochou-Lishan fault (CLF). The Longitudinal Valley (LV) suture is located in the east side of the CR. The inset shows the epicenter of the 2005 Mw8.6 Nias earthquake and the great circle path to the study region (square).

arrival times for the rest of the stations within 50 km of the LFE source.

[7] After obtaining initial hypocenters of 11 LFEs, we used seismic data 3 s before and after the S-wave arrivals of each LFE as waveform templates, and scanned through the 700 s data to detect additional LFEs [*Brown et al.*, 2008, 2009; *Peng and Zhao*, 2009]. We calculated the correlation coefficient (CC) values for the two horizontal components at all stations, and computed a network averaged CC values for each time window that steps forward at 0.05 s (1 sample). Next, we applied a threshold based on the median absolute deviation (MAD) of the averaged CC values to identify new events. Following *Brown et al.* [2008], we saved all window pairs that exceed our detection threshold of 5 times the MAD. A total of 30 new events are detected.

[8] We then used the matched filter technique again to help identify the P- and S-wave arrivals of the 30 new LFEs (Figure 2b). The window length of the original template LFEs is decreased to be 4-s with 2 s before and after the S-wave arrivals. We appended 2 s (1 s before and after) to each time segment of the 30 new LFEs so that the time window now becomes 8 s. Then the 4-s waveforms of the original 11 LFEs are used to scan through the 8-s time segment of the 30 new events to detect their S-wave arrivals with the threshold of 10 times the MAD. Similarly, we appended 1 s before and after each time segment and used the same procedure to search for the P-wave arrivals. Next, we computed the differential travel times of P and S waves

based on the 4-s time window centered on the detection time. Figure S7 shows two examples of aligned P and S waves recorded at stations ALS and CHN4. The alignments on the vertical and horizontal components correspond to the P and S-wave arrivals, respectively. When the P wave is aligned on the vertical component, the S-wave energy is barely visible. Similarly, when we align the S wave on the horizontal component, the P wave is not clearly shown. This means that the S-P times of the LFEs are slightly different, suggesting that these LFEs occur in slightly different locations.

[9] Finally, we relocate all the LFEs based on the new 1-D average velocity model and the cross-correlated differential travel times [*Waldhauser and Ellsworth*, 2000]. Because the LFE and tremor signals are better shown in the horizontal components as S waves than in the vertical component as P waves, we set the weighting factor of 0.7 for the S waves and 0.3 for the P waves. The locations of the LFEs are slightly different if we set different weighting factors, but the changes are minor. In addition, we required at least 5 stations with both P and S-wave arrivals for each LFE to ensure reliable location.

3. Results

[10] Figure 1 shows the epicenters of the LFEs and the corresponding depth profile is shown in Figure 3. It is clear from both plots that the LFEs are located close to the Chaochou-Lishan fault (CLF), which is a high-angle thrust fault with minor strike-slip component beneath the CR [*Ho*, 1986; *Tillman and Byrne*, 1995]. These events are distributed at depth from ~12 to 38 km, just below the depth range of regular earthquakes (Figure 3c). Both the horizontal and vertical errors are less than 1.5 km. A recent study based on receiver functions has shown that the deepest Moho depth is below the CR (C.-C. Tang et al., Variation of Moho depth in Taiwan area from radial receiver functions and its tectonic implication, submitted to *Geophysical Journal International*, 2010) and most LFEs are just above the deepest Moho depth. In addition, most LFEs appear to be on or near the downdip extent of the high-angle CLF, although the LFEs do not collapse into a single planar structure. If we used the previous 1D velocity model of central Taiwan [*Chen et al.*, 2001], the depths of the LFEs are slightly deeper, but the main structural feature remains similar (Figure S8). In Figures 3a and 3b we also plotted the P-wave velocity and the Vp/Vs ratio from the recent 3-D seismic tomography [*Wu et al.*, 2007]. We find that the locations of LFEs coincide with a region with relatively high Vp/Vs ratio (1.75–1.85). The highest Vp/Vs ratio (>1.85) is close to the Longitudinal Valley (LV) suture to the east, which is a NNE-striking boundary that separates the Chinese continental margin and the Luzon Arc.

4. Interpretation

[11] Taiwan is a result of ongoing collision between the Philippine Sea Plate and the Eurasian Plate [*Ho*, 1986; *Teng*, 1990]. This ongoing process causes two subduction zones northeast and southeast of Taiwan and several significant large-scale fault systems (mainly thrust with a minor strike-slip component) in Taiwan. Although the CLF is a main suture that separates the Slate Belt from the CR [*Tillman*
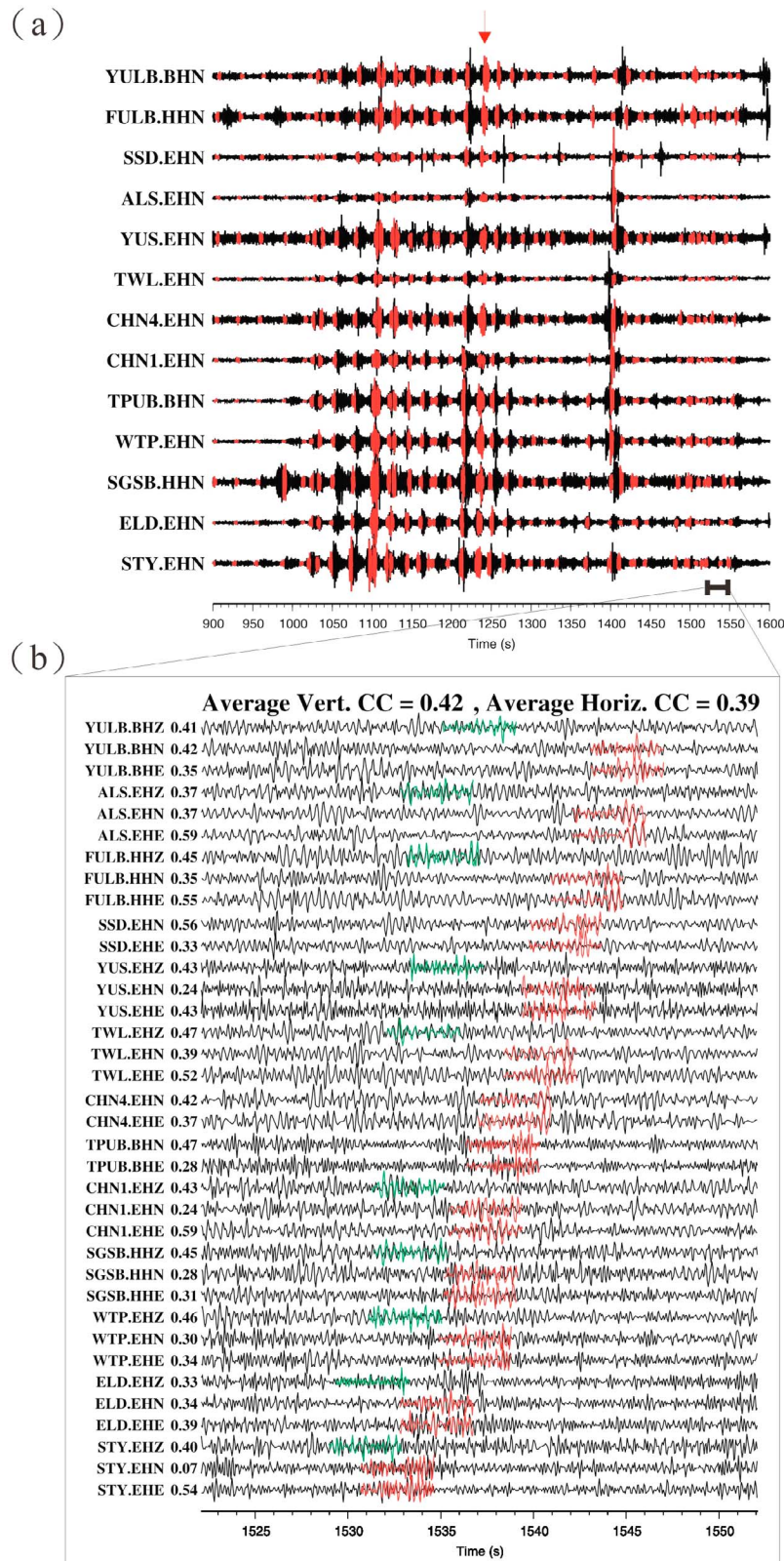
Figure 2. (a) The 2–8 Hz band-pass-filtered north-component seismograms showing tremor triggered by the Nias earth-quake. Red segments represent 2 s before and after the theoretical S-wave arrivals of the 41 LFEs detected in this study. The seismograms are plotted from the bottom to top with increasing epicentral distances to the centroid of 41 LFEs. The red arrow indicates the time segment of the template shown in Figure 2b. (b) An example showing the waveform detection of the P (green lines) and S (red lines) waves of a new LFE based on an template occurred at around 1535 s. Individual CC value is shown on the left side and the average CC values for vertical and horizontal component are shown on the top.
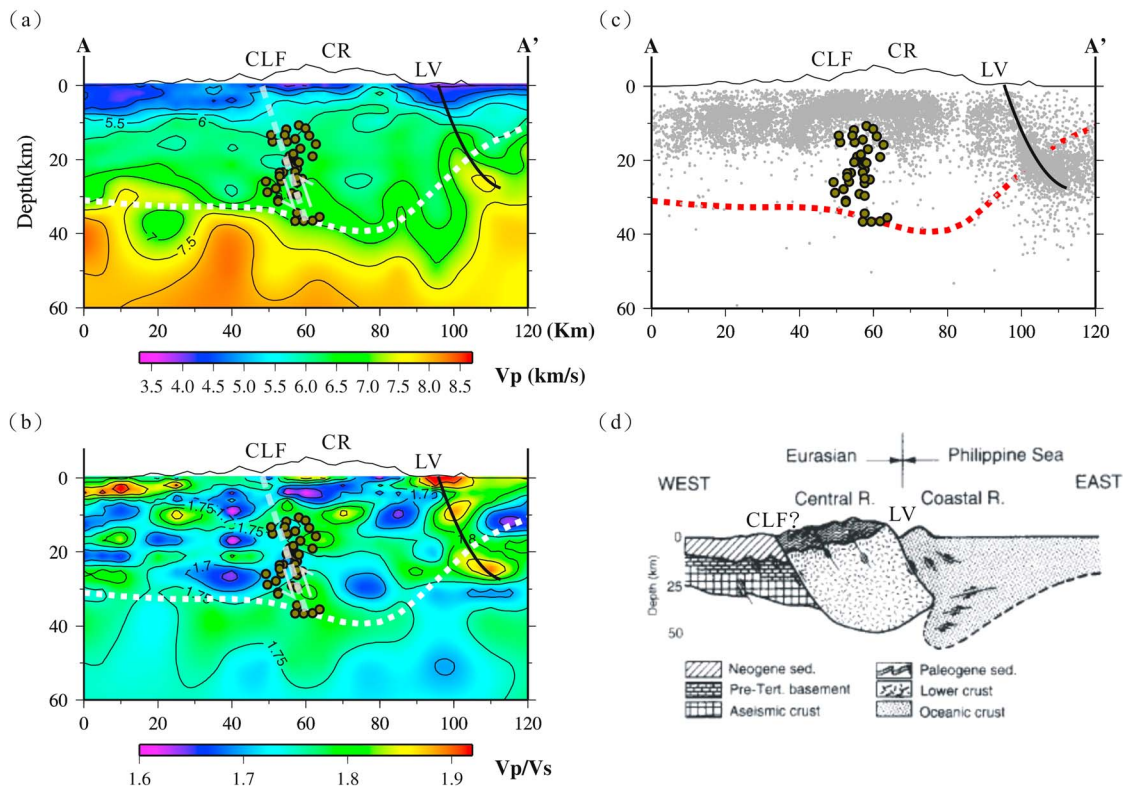
Figure 3. (a) Locations of LFEs plotted on top of the Vp velocity model of *Wu et al.* [2007], (b) the Vp/Vs profile, and (c) the background seismicity from 1991 to 2008 along the AA' projection shown in Figure 1. The while dotted lines show the variation of the Moho depth (C.-C. Tang et al., submitted manuscript, 2010) with error of ~3 km in vertical direction. CLF, Choachou-Lishan Fault; LV, Longitudinal Valley suture. The black solid line indicates a possible dipping direction of the LVF. The thick gray dashed line represents the depth extension the CLF. The lines above 0 km mark the topography along AA'. (d) A simple illustration of the Lithospheric Collision Model. Modified from *Wu et al.* [1997].

and Byrne, 1995], its role in the mountain building process of Taiwan is still in debate. *Suppe* [1981] proposed a thin-skinned tectonics model, in which a decollement interface dipping about 6–10 degrees is responsible for accommodating the shortening between the two colliding plates. Alternatively, *Wu et al.* [1997] suggested a Lithospheric Collision Model to explain the tectonics of Taiwan across the CR (Figure 3d). In this model, the Eurasian Plate and the Philippine Sea Plate are colliding in eastern Taiwan and the crust shortens and thickens in central Taiwan without the basal detachment. They also proposed that a boundary beneath the CR separates the crust into two different geological units. Based on the locations and the dip of the CLF, we suggest that the CLF could be this boundary that extends down to the Moho discontinuity at depth. The triggered LFEs mainly occur on the downward extension of the CLF below the background seismicity (Figure 3c), rather than illuminating a near-horizontal detachment as suggested by the previous study [*Peng and Chao*, 2008]. However, it is worth mentioning that the LFE locations obtained here are only associated with one triggered tremor episode (700 s). In addition, several recent studies have shown that triggered and ambient tremors do not always originate in the same locations [e.g., *Peng et al.*, 2009; *Rubinstein et al.*, 2010]. Hence, we cannot rule out the possibility that tremor and

LFEs could occur at other locations and faults in Southern Taiwan.

5. Discussion and Conclusion

[12] Many recent studies have shown that tremor and LFEs occur in a region with elevated fluid pressures [e.g., *Rubinstein et al.*, 2010; *Peng and Gomberg*, 2010, and references therein]. It is generally accepted that near-lithostatic fluid pressures would reduce the effective confining pressures and hence result in extremely weak faults that slip during tremor and/or slow-slip events. In the subduction zone environment, aqueous fluids mainly come from dehydration of hydrous minerals within the subducting sediments [*Peacock*, 2009]. In the collision environment here, fluids could come from metamorphic or dehydration reaction in the lower crust/upper mantle [*Suppe*, 1981]. Previous magnetotelluric (MT) studies beneath the CR have revealed the existence of a high conductivity zone in the lower crust [e.g., *Chen and Chen*, 1998], and suggested a link between the high conductivity zone and fluids from dehydration reactions. Here we found that the LFEs are close to a region around the downward extension of the CLF with relatively high Vp/Vs ratio (1.75–1.85) from the 3D seismic tomography [*Wu et al.*, 2007]. However, the region outlined by the

LFEs does not have anomalously high Vp/Vs ratio as compared with the surrounding regions. Instead, the highest Vp/Vs ratio, and presumably the most elevated fluid pressures occur near the LV suture, which is partially creeping in the shallow crust [*Lee et al.*, 2001] with numerous small earthquakes, occasionally large (M6-7) earthquakes, and slow-slip events [e.g., *Liu et al.*, 2009]. So far, no tremor and LFEs have been detected near the LV suture. Hence, we suggest that elevated fluid pressures would help, but is not the only requirement for tremor and LFE generation. It is also possible that resolution of the current tomography results [*Wu et al.*, 2007] might not be high enough to reveal the existence of high fluid pressure near the CLF. Further refined tomographic imaging studies in this region could help to resolve this issue.

[13] As briefly mentioned before, the obtained LFE locations and the tectonic interpretation are slightly different from those of *Peng and Chao* [2008]. In that study, they obtained a tremor depth of 19 km, which is near the top of the most LFEs indentified in this study (Figure 3). Based on the correlations between the tremor burst and Love wave displacement, they suggested that the triggered tremor was generated by shear slip on the weak detachment fault beneath the CR in Southern Taiwan. The main difference stems from the fact that *Peng and Chao* [2008] treated the peaks of the envelope functions as S-wave arrivals and used them to locate the tremor, assuming that all triggered tremor bursts come from the same region. In reality, a tremor burst may be a superposition of many LFEs that come from slightly different locations [e.g., *Shelly et al.*, 2007; *Shelly*, 2010]. In addition, the envelope-based location procedure only utilized the S-arrival information, while the LFE-based location procedure used both P and S-wave arrivals. Hence in principle, the LFE approach should result in better locations, especially the depth.

[14] One limitation of the matched filter technique is that the seismic signal needs to be similar to the template in order to be detected. In this study we only have 11 LFE templates with high SNR. It is possible that more LFEs can be detected if we use more template events, or an autocorrelation approach [*Brown et al.*, 2008, 2009] is employed. Our results, together with other recent studies of LFEs [*Brown et al.*, 2008, 2009; *Shelly et al.*, 2007; *Shelly*, 2010] suggest that at least of part of the triggered tremor consists of LFEs. These LFEs probably represent shear failure on or near the major fault interface, just like ambient and triggered tremor that occurred in Taiwan [*Peng and Chao*, 2008; K. Chao et al., submitted manuscript, 2010] and elsewhere [*Shelly et al.*, 2007; *Peng et al.*, 2009]. We have examined but found no discernable temporal evolutions of the LFE locations during the passage of the surface waves. Hence, it is still not clear whether the triggered tremor and LFEs represent slow-slip events triggered by teleseismic events [*Peng et al.*, 2009]. Further studies are needed to verify their focal mechanisms, and understand their relationship to the ambient conditions, slow-slip and other tectonic processes beneath the CR.

[15] Tremor is now widely observed along major plate-boundary faults and is providing new information about the fault slip behaviors at the deep roots of fault zones [*Rubinstein et al.*, 2010; *Peng and Gomberg*, 2010]. As mentioned before, tremor and LFEs are extremely stress sensitive and hence could act as a natural 'stress meter' to monitor time-dependent changes around deep faults, especially before large earthquakes [*Shelly*, 2010]. Because Taiwan is seismically active with frequent occurrence of damaging earthquakes, continuous monitoring of tremor and LFEs would not only help to better understand the deep extension of active faults in Taiwan, but also has a great potential for deciphering time-dependent changes during large earthquake cycles and hence contributing to seismic hazard mitigation in this region.

References

Brown, J. R., G. C. Beroza, and D. R. Shelly (2008), An autocorrelation method to detect low frequency earthquakes within tremor, *Geophys. Res. Lett.*, 35, L16305, doi:10.1029/2008GL034560.

Brown, J. R., G. C. Beroza, S. Ide, K. Ohta, D. R. Shelly, S. Y. Schwartz, W. Rabbel, M. Thorwart, and H. Kao (2009), Deep low-frequency earthquakes in tremor localize to the plate interface in multiple subduction zones, *Geophys. Res. Lett.*, 36, L19306, doi:10.1029/2009GL040027.

Chen, C.-C., and C.-S. Chen (1998), Preliminary result of magnetotelluric soundings in the fold-thrust belt of Taiwan and possible detection of dehydration, *Tectonophysics*, 292, 101–117, doi:10.1016/S0040-1951 (98)00059-6.

Chen, C.-H., W.-H. Wang, and T.-L. Teng (2001), 3D velocity structure atound the source area of the 1999 Chi-Chi, Taiwan, Earthquake: Before and after the mainshock, *Bull. Seismol. Soc. Am.*, 91, 1013–1027, doi:10.1785/0120000737.

Gibbons, S. J., and F. Ringdal (2006), The detection of low magnitude seismic events using array-based waveform correlation, *Geophys. J. Int.*, 165, 149–166, doi:10.1111/j.1365-246X.2006.02865.x.

Ho, C. S. (1986), A synthesis of the geologic evolution of Taiwan, *Tectonophysics*, 125, 1–16, doi:10.1016/0040-1951(86)90004-1.

Kao, H., S.-J. Shan, H. Dragert, and G. Rogers (2009), Northern Cascadia episodic tremor and slip: A decade of tremor observations from 1997 to 2007, *J. Geophys. Res.*, 114, B00A12, doi:10.1029/2008JB006046.

Lee, J.-C., J. Angelier, H.-T. Chu, J.-C. Hu, and F.-S. Jeng (2001), Continuous monitoring of an active fault in a plate suture zone: a creepmeter study of the Chihshang Fault, eastern Taiwan, *Tectonophysics*, 333, 219–240, doi:10.1016/S0040-1951(00)00276-6.

Liu, C.-C., A. T. Linde, and I. S. Sacks (2009), Slow earthquakes triggered by typhoons, *Nature*, 459, 833–836, doi:10.1038/nature08042.

Obara, K. (2002), Nonvolcanic deep tremor associated with subduction in southwest Japan, *Science*, 296, 1679–1681, doi:10.1126/science. 1070378.

Peacock, S. M. (2009), Thermal and metamorphic environment on subduction zone episodic tremor and slip, *J. Geophys. Res.*, 114, B00A07, doi:10.1029/2008JB005978.

Peng, Z., and K. Chao (2008), Non-volcanic tremor beneath the Central Range in Taiwan triggered by the 2001 Mw 7.8 Kunlun earthquake, *Geophys. J. Int.*, 175(2), 825–829, doi:10.1111/j.1365-246X.2008. 03886.x.

Peng, Z., and J. Gomberg (2010), An integrated perspective of the continuum between earthquakes and slow-slip phenomena, *Nat. Geosci.*, doi:10.1038/ngeo940.

Peng, Z., and P. Zhao (2009), Migration of early aftershocks following the 2004 Parkfield earthquake, *Nat. Geosci.*, 2, 877–881, doi:10.1038/ ngeo697.

Peng, Z., J. E. Vidale, A. Wech, and R. M. Nadeau (2009), Remote triggering of tremor along the San Andreas Fault in central California, *J. Geophys. Res.*, 114, B00A06, doi:10.1029/2008JB006049.

Rogers, G., and H. Dragert (2003), Episodic tremor and slip on the Cascadia subduction zone: The chatter of silent slip, *Science*, 300, 1942–1943, doi:10.1126/science.1084783.

Rubinstein, J. L., J. E. Vidale, J. Gomberg, P. Bodin, K. C. Creager, and S. D. Malone (2007), Non-volcanic tremor driven by large transient shear stresses, *Nature*, 448, 579–582, doi:10.1038/nature06017.

Rubinstein, J. L., D. R. Shelly, and W. L. Ellsworth (2010), Non-volcanic tremor: a window into the roots of fault zones, in *New Frontiers in Integrated Solid Earth Sciences*, edited by S. Cloetingh and J. Negendank, pp. 287–314, Springer, New York.

Shelly, D. R. (2010), Migrating tremors illuminate complex deformation beneath the seismogenic San Andreas fault, *Nature*, *463*, 648–652, doi:10.1038/nature08755.

Shelly, D. R., G. C. Beroza, and S. Ide (2007), Non-volcanic tremor and low frequency earthquake swarms, *Nature*, *446*, 305–307, doi:10.1038/nature05666.

Suppe, J. (1981), Mechanics of mountain building and metamorphism in Taiwan, *Mem. Geol. Soc. China*, *4*, 67–89.

Teng, L.-S. (1990), Geotectonic evolution of late Cenozoic arc-continent collision in Taiwan, *Tectonophysics*, *183*, 57–76, doi:10.1016/0040-1951(90)90188-E.

Tillman, K. S., and T. B. Byrne (1995), Kinematic analysis of the Taiwan Slate Belt, *Tectonics*, *14*, 322–341, doi:10.1029/94TC02451.

Waldhauser, F., and W. L. Ellsworth (2000), A double-difference earthquake location algorithm: Method and application to the northern Hayward fault, *Bull. Seismol. Soc. Am.* *90*13531368 doi:10.1785/0120000006.

Wu, F. T., R. J. Rau, and D. Salzberg (1997), Taiwan orogeny: Thin-skinned or lithospheric collision?, *Tectonophysics*, *274*, 191–220, doi:10.1016/S0040-1951(96)00304-6.

Wu, Y.-M., C.-H. Chang, L. Zhao, J. Bruce, H. Shyu, Y.-G. Chen, K. Sieh, and J.-P. Avouac (2007), Seismic tomography of Taiwan: Improved constraints from a dense network of strong motion stations, *J. Geophys. Res.*, *112*, B08312, doi:10.1029/2007JB004983.

K. Chao and Z. Peng, School of Earth and Atmospheric Sciences, Georgia Institute of Technology, 311 Ferst Dr., Atlanta, GA 30332, USA.

C.-H. Chen and C.-C. Tang, Institute of Seismology, National Chung Cheng University, 168 University Rd., Min-Hsiung, Chia-Yi County 62102, Taiwan.

C.-H. Lin, Institute of Earth Sciences, Academia Sinica, 128, Sec. 2, Academia Rd., Nangang, Taipei 11529, Taiwan.